Hindawi
Scientific Programming
Volume 2022, Article ID 1509490, 9 pages
https://doi.org/10.1155/2022/1509490

Research Article

Convolutional Neural Network in Evaluation of Radiotherapy Effect for Nasopharyngeal Carcinoma

Haifeng Qian[1] **and Yancheng Fang**[2]

[1]*Imaging Center, The Third Affiliated Clinical Hospital of Changchun University of Chinese Medicine, Changchun 130117, Jilin, China*
[2]*Department of Radiology, Shenzhen Stomatology Hospital (Pingshan) of Southern Medical University, Shenzhen 518000, Guangdong, China*

Correspondence should be addressed to Yancheng Fang; 1618403011@stu.suda.edu.cn

Received 27 September 2021; Revised 25 November 2021; Accepted 11 January 2022; Published 31 January 2022

Academic Editor: M Pallikonda Rajasekaran

This study was aimed to explore the adoption value of magnetic resonance imaging (MRI) under convolutional neural networks (CNN) in the therapeutic effect of nasopharyngeal carcinoma (NPC) radiotherapy. A total of 54 NPC patients were recruited. CNN was employed to perform 3D visualization processing on magnetic resonance (MR) images of NPC patients. MRI changes were analyzed before and after the patient received radiotherapy. The image segmentation and radiotherapy effects of CNN were evaluated by the Recall, intersection over union (IOU), postoperative apparent diffusion coefficient (ADC), and diagnostic coincidence rate. Moreover, gradient vector flow (GVF) algorithm, fuzzy c-means (FCM), and SegNet were adopted for comparative evaluation. Recall of CNN was 94.89% and the IOU was 84.16%, which was remarkably different from other algorithms ($P < 0.05$). After analysis of the MRI images of patients receiving radiotherapy, ADC of local residual patients was 1.108 ± 0.097 measured by CNN, the ADC was 1.826 ± 0.115, and the missed diagnosis rate was only 7.14%. In summary, CNN had a good effect on the localization and segmentation of NPC patients, and can accurately evaluate the effect of patients receiving radiotherapy, which can assist clinical diagnosis and treatment of NPC.

1. Introduction

Nasopharyngeal carcinoma (NPC) is a malignant tumor in the mucosa of the nasopharynx. Its occurrence is obviously regional [1, 2]. Most NPC patients are often accompanied by neck mass. In addition, they are prone to hearing loss, tinnitus, earache, and recurrent ear infection [3]. The incidence of NPC is the first among head and neck malignant tumors. With the gradual development of radiotherapy technology, NPC has been controlled to a certain extent. Patients who receive radiation therapy typically have their lesions completely gone within three months. If the tumor does not disappear six months after surgery, it is residual tumor, and NPC residual or recurrence is the main reason that affects the prognosis and quality of life of patients. At present, the screening of NPC mainly includes imaging examination and detection of NPC virus infection in blood, including computerized tomography (CT) and magnetic resonance imaging (MRI) [4]. Its treatments are classified into local treatment (radiotherapy and surgery) and systemic treatment (chemotherapy, targeted therapy, immunotherapy, etc.) [5]. NPC is very sensitive to radiotherapy, and radiotherapy is the main treatment for NPC. In the early stage, only radiotherapy is utilized, and radiotherapy is mainly combined treatment in the local late stage [6]. With the popularization of intensity-modulated radiation therapy technology and the adoption of comprehensive treatment, the NPC local control rate is more than 90%, and the 5-year survival rate is more than 80%. In contrast to other tumors, NPC treatment has objective efficacy [7, 8].

At present, CT and MRI are commonly applied for the clinical diagnosis of NPC [9]. CT technology gives a lower

resolution of soft tissue images, whereas MRI can clearly show the tumor site, invasion range, and lymph node metastasis [10]. In contrast to CT, MRI can remarkably increase the detection rate of soft tissue invasion around nasopharynx by about 30% and the detection rate of bone invasion at skull base by 20%. In addition, the detection rates of skull base invasion and parapharyngeal space invasion were remarkably improved [11, 12]. With breakthrough of medical imaging, the revolution of CT and MRI are enhanced, which provide good help for doctors in diagnosis and treatment [13]. CT has high density resolution, which can clearly show the patient's anatomical relationship, and the clinical examination is quick. However, because of its large radiation amount and only cross-sectional scan, its use is limited. MRI is utilized to evaluate the efficacy of NPC radiotherapy due to its omni-directional and multi-parameter characteristics, which can accurately reflect the nerves and blood vessels at the lesion site. The quantification technology of image processing is actually very critical, which plays an important role in disease diagnosis and early prevention [14]. Now many quantitative analyses are a segmentation problem, and effective and automatic organ region segmentation is very challenging. The brightness difference between different parts is not obvious, connected with the surrounding parts, and the boundary is fuzzy. In addition, there are noise and other interference factors [15, 16]. Deep learning convolutional neural networks (CNN), cyclic neural networks, generative adversarial networks, etc. can focus on medical image imaging problems. In recent years, computer-aided medical image analysis has made major breakthroughs in technology and has obvious advantages in improving the efficiency and ability of medical services [17], which has also become an effective way to solve problems such as insufficient medical resources.

Therefore, it was attempted to build a CNN model, train the network to segment the MRI image of NPC, and conduct three-dimensional visualization of the MRI image, to make the image stereoscopic display. After training, CNN was utilized to segment NPC MRI images, to comprehensively study the adoption value of MRI based on CNN deep learning algorithm in the evaluation of therapeutic effect of diagnostic NPC radiotherapy. Moreover, further reference and basis were offered for the adoption of CNN in the diagnosis and curative effect evaluation of NPC.

2. Methods

2.1. Samples. In this study, 42 patients with NPC who visited hospital from March 2019 to March 2021 were recruited. There were 23 male patients and 19 female patients in total, with the average age of 55.2 ± 11.3 years old. All patients were diagnosed pathologically and graded into $T_1N_0M_0$ of 7 cases, $T_{1\text{-}2}N_1M_0$ of 7 cases, $T_2N_0M_0$ of 5 cases, $T_{1\text{-}3}N_2M_0$ of 7 cases, $T_3N_{0\text{-}2}M_0$ of 5 cases, $T_3N_1M_0$ of 4 cases, $T_4N_2M_0$ of 4 cases, and $T_2N_2M_0$ of 3 cases according to the Tumor Node Metastasis (TNM) staging established by American Joint Committee on Cancer. The details of TNM standard are shown in Table 1. All patients underwent radiotherapy, followed by MRI examination before and after radiotherapy. The target area and normal organs were delineated based on MRI images, and radiotherapy was implemented based on the delineation results. All patients had signed the informed consent forms and this study had been approved by the ethics committee of hospital.

Inclusion criteria: (i) those confirmed as NPC by pathological biopsy before radiotherapy; (ii) patients aged between 18 and 70 years; (iii) the patient had no previous tumor history; (iv) patients who were able to participate in the study and follow-up; (v) no serious metabolic diseases such as heart, brain, and kidney.

Exclusion criteria: (i) biopsy pathology was not clear; (ii) the patient had contraindications to radiotherapy and chemotherapy and MRI.

2.2. MRI Examination. Magnetic Resonance Imaging System was employed to perform MRI scans on 42 NPC patients. The patient was in a supine position, and the cross-sectional, sagittal, and coronal planes of the patient were scanned using standard head coils and spin echo sequences. The T1 weighted imaging (T1WI) scan sequence was utilized for the transverse and coronal planes, and the T1WI and T2 weighted imaging (T2WI) scan sequences were utilized for the sagittal plane. Time of inversion (TI): 110 ms, time of echo (TE): 48 ms, time of repetition (TR): 3,800~5,100 ms, layer spacing: 6 mm, layer thickness: 5 mm, and flip angle: 90°.

2.3. Radiotherapy. Radiation therapy was performed on all NPC patients participating in this study. Before treatment, the clinical target volume (CTV) of the patients was delineated according to MRI. High-risk CTV1 included the parapharyngeal space, slope, rupture hole, and lymphatic drainage area where the positive lymph nodes in the neck were located. Low-risk CTV2 included low-risk lymphatic drainage areas where subclinical metastasis may occur. After the delineation was over, each target area was expanded back by 2–3 mm, and expanded 3–4 mm outside of other directions to be the planned target volume. During radiotherapy, 6MV-X linear accelerator was utilized for external irradiation, the irradiated skin area was $100\,\text{mm} \times 125\,\text{mm}$~$130\,\text{mm} \times 160\,\text{mm}$, the dose was 6,000~7,000 Gy, and the course of treatment was 45~65 days.

2.4. Construction of NPC Radiotherapy Curative Effect Model under CNN. NPC radiotherapy efficacy evaluation including data preprocessing and CNN model was completed. Data need to be normalized as the dimension between the features in the actual prediction is different. Normalization of maximum and minimum values is adopted to standardize the data.

$$x = \frac{x_0 - x_{\min}}{x_{\max} - x_{\min}}. \tag{1}$$

In equation (1), x is data after normalization of maximum and minimum, x_0 is pre-processed data, $x_{\max}$ is the maximum of dimensional data, and $x_{\min}$ is the minimum. It

Table 1: Staging criteria for NPC.

Staging	Indexes
T: primary tumor	
TX	Primary tumor cannot be evaluated
T0	There is no evidence of primary tumor, including EBV positive in cervical lymph nodes
T1	The tumor is confined to the nasopharynx, or invades the oropharynx and/or nasal cavity
T2	The parapharyngeal space and/or adjacent soft tissues are invaded, including the internal pterygoid muscles, the external pterygoid muscles, and the anterior vertebral muscles
T3	The skull base, cervical vertebrae, pterygoid structure, and/or paranasal sinuses are invaded
T4	Intracranial tumor invasion is found; and invasion of cranial nerves, hypopharynx, orbits, parotid glands, and/or soft tissue infiltration of lateral margin of pterygoid muscle are observed
N: regional lymph node	
NX	Regional lymph nodes cannot be evaluated
N0	No regional lymph node metastasis is found
N1	There is unilateral cervical lymph node metastasis, and/or unilateral/bilateral retropharyngeal lymph node metastasis. The maximum diameter of the metastasis is ≤6 cm, and the metastasis occurs above the lower edge of the cricoid cartilage
N2	Bilateral cervical lymph node metastasis is found. The maximum diameter of the metastasis is ≤6 cm, and the metastasis is above the lower edge of the cricoid cartilage
N3	Unilateral or bilateral cervical lymph node metastasis is found. The maximum diameter of the metastasis is >6 cm, and/or the invasion exceeds the lower edge of the cricoid cartilage
M: metastasis	
M0	No metastasis
M1	Metastasis

is necessary to reduce the dimension of data to speed up the training. The data redundancy information is presented by principal component analysis. If matrix H contains a samples, and b is row vector of different attributes of each sample, then the matrix H is expressed as follows:

$$\begin{aligned} H &= \left(H_1, H_2, H_3, \cdots, H_a\right), \\ H_1 &= \left(h_1^1, h_2^1, h_3^1, \cdots, h_b^1\right)^T. \end{aligned} \tag{2}$$

Column vector of H is P, then $P = (P_1, P_2, P_3, \cdots, P_b)^T$. The covariance is obtained regarding different P, and a matrix G is formed.

$$G(m,n) = \operatorname{cov}\left(P_m, P_n\right) = E\left[\left(p_m - c_m\right) * \left(p_n + c_n\right)\right]. \tag{3}$$

c_m and c_n are expectations of P_m and P_n, respectively. Matrix element values reflect linear correlation degree between two random variables. Two random variables are linearly independent with covariance of 0. Large covariance reflects strong correlation. H is transformed to harvest transformation matrix of H to calculate eigenvalues and eigenvectors of H. Large feature value means large numerical range and variance of it in data compression. The transformation matrix is constructed by using the eigenvectors corresponding to large eigenvalues to obtain new features of high importance.

After data treatment, CNN model is utilized to evaluate the curative effect of NPC radiotherapy. The convolution layer includes convolution, activation, and pooling. After the original data is input, feature mapping is performed on the data obtained after the original data is convolved with the convolution kernel (CK). The calculation of neural network on 2D tensors is shown as below.

$$y[\overline{m}, \overline{n}] = \sum_i \sum_l x[\overline{m} + i, \overline{n} + l] w[i, l]. \tag{4}$$

$y[\overline{m}, \overline{n}]$ is output 2D tensor, $x[\overline{m}, \overline{n}]$ is input 2D tensor, and $w[i, l]$ is CK's weight. Each layer in a complete CNN contains several feature images. If each layer contains a CK, and each CK is composed of massive parameters, the convolution is implemented for each layer as follows.

$$y_{\overline{n}}^s = \sum_{i=1}^{A} w_{\overline{n}i}^s y_i^{s-1} + c_{\overline{n}}^s. \tag{5}$$

In equation (5), $\overline{n}$th feature image of s-th layer convolution is $y_{\overline{n}}^s$, and CK parameter of i-th feature image of $s-1$th convolution layer mapped to the $\overline{n}$th feature image of s-th layer convolution is $w_{\overline{n}i}^s$. i-th feature image of $s-1$th CL is y_i^{s-1}, and offset of $\overline{n}$th feature image of s-th CL is $c_{\overline{n}}^s$. Convolution refers to linear transformation. Usually, multilayer nonlinear feature is formed with a nonlinear activation function after convolution of all layers. Taking the sigmoid function as an example, the expression is as follows:

$$f(x) = \frac{1}{e^{-x} + 1}. \tag{6}$$

Without performing weighting or requiring activation functions, pooling performs maximum or average operations to express statistical characteristics of the pooling results. It is only involved in network institution design to reduce data dimensions, speed up calculations, and avoid over-fitting (Figure 1).

Through the full connection layer, image is transmitted to the output layer after original features extraction through the CL and main features from the sub-sampling layer. The full

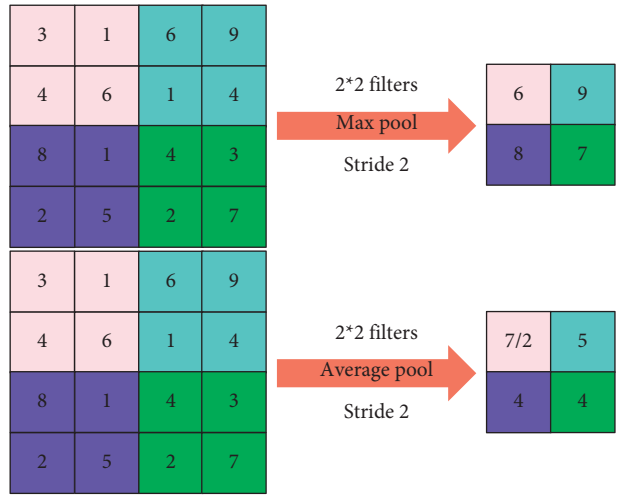

Figure 1: Two kinds of pooling.

connection layer maps the information processed by CL and sub-sampling layer to the label space of the sample. 2D feature graph is converted into 1D feature vector, and the information is summarized for full-neural network training (Figure 2). Different from CL, the fully connected layer captures the nonlinear relationship between CL's comprehensive feature information and sub-sampling layer to learn feature information, to accurately classify features.

In the process of calculating CNN, in order to prevent the model from over-fitting due to the excessive feature information contained in the full connection layer, it is usually necessary to introduce the normalized function to carry out the final classification. The final classification layer utilized is Softmax function in this work. The classification function is as follows:

$$\sigma(u) = \frac{e^u}{\sum_{K=1}^{K} e^j}. \tag{7}$$

In equation (7), probability of a sample in a category is σ, output of the neuron is u, and number of categories is K.

2.5. Evaluation Indexes. When NPC lesions were detected, the results obtained by subjective judgment alone were unreliable. Therefore, segmentation results of CNN were objectively evaluated regarding recall and intersection over union (IOU). GVF, FCM, and SegNet were adopted for comparison. The function expressions of Recall and IOU are as follows:

$$Recall = \frac{\mathrm{TP}}{\mathrm{FN} + \mathrm{TP}}, \tag{8}$$

$$IOU = \frac{|S \cap S_0|}{||S \cup S_0||}. \tag{9}$$

In equations (8) and (9), TP represents the pixels of the positive lesions in the area delineated by the algorithm, FN represents the pixels of the positive lesions outside the area delineated by the algorithm, S is the area delineated by the algorithm, and S_0 is the area delineated by the expert [18–20].

2.6. Statistical Treatment. SPSS 22.0 was employed. Count data were expressed in the form of %, quantitative data are represented by ($\overline{x} \pm s$), tested by χ^2 test. t-test was utilized between independent samples. $P < 0.05$ meant considerable differences.

3. Results

3.1. MRI Image Preprocessing of NPC Patients. Due to the limitation of MRI imaging, as well as the inhomogeneity of the magnetic field or the movement of the patient during the imaging process, it is easy to cause the image to produce motion artifacts, noise, and blurred edges. Therefore, the image was pre-processed for image enhancement to highlight image features and prepare for the next step of lesion segmentation. The preprocessing result is shown in Figure 3. The patient's nasopharyngeal cavity was narrowed, and the nasopharyngeal mucosa on the right side was swollen and distributed asymmetrically. Due to the noise artifacts in the original image, the image was smoothed and gray-scale adjusted.

3.2. NPC Lesion Detection Model Based on CNN. The CNN was utilized to locate the NPC lesion area, then this area was delineated and segmented, and the segmented image area was reduced at the same time. When the lesion area was delineated, manual delineation required the doctor to observe the scope of the lesion carefully and comprehensively on the MRI image and delineate the tumor target area layer by layer. Therefore, the results obtained only by the subjective judgment of clinicians were often unstable. When CNN was adopted for detection, the detection results were adjusted to make the results stable. In Figure 4, the blue area was the NPC lesion area outlined by the radiologist, and the red area was the area automatically segmented by CNN. Notably, the lesion area marked by CNN was relatively more accurate, which was similar to the expert's outline of the lesion.

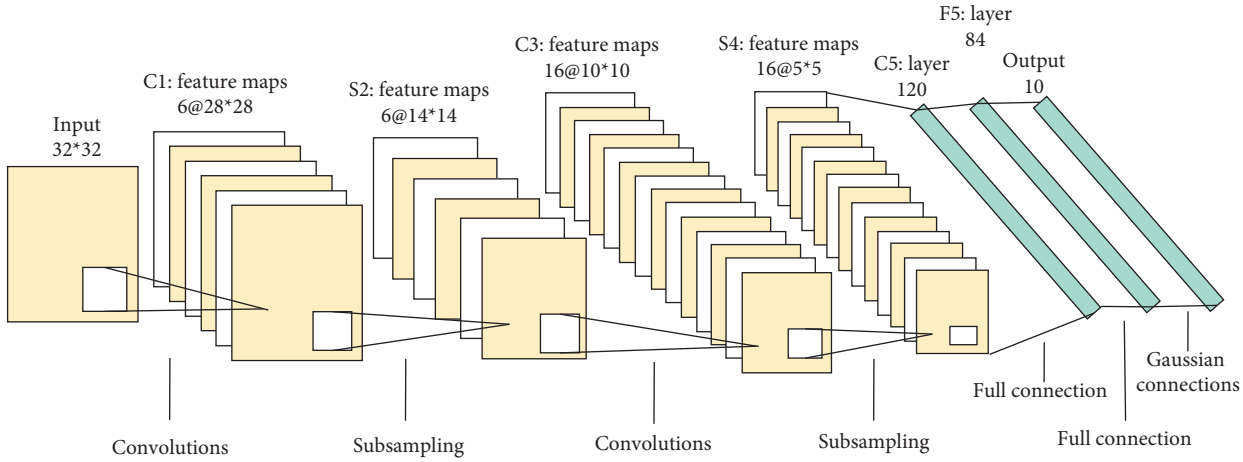

Figure 2: Schematic diagram of CNN.

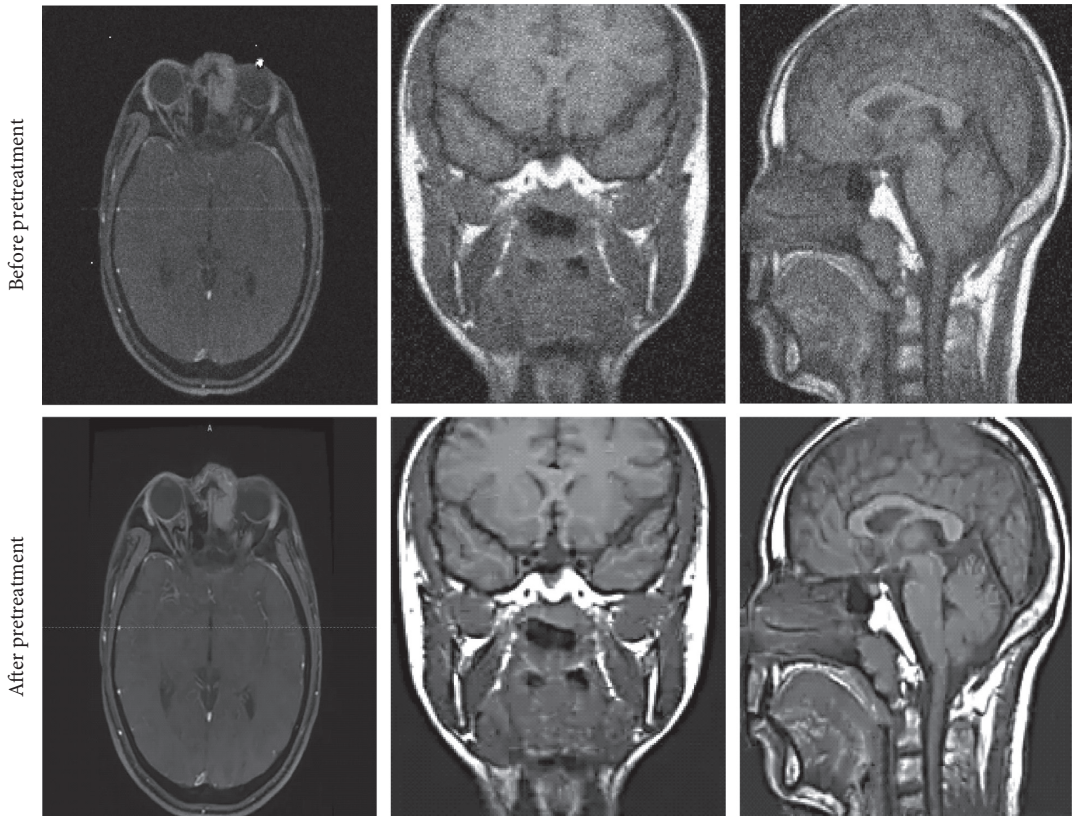

Figure 3: Schematic diagram of preprocessing results of MRI images of NPC patients.

In addition to subjective evaluation, segmentation effect of CNN was objectively evaluated regarding Recall and IOU. The results are shown in Figure 5. In contrast to other algorithms, it was found that the Recall and IOU of CNN were 94.89% and 84.16%, respectively. The Recall and IOU of the GVF were 67.48% and 52.15%, respectively. Those of the FCM were 84.12% and 68.71%, respectively. The Recall and IOU of the SegNet were 78.44% and 65.01%, respectively. After the image was pre-processed in the initial stage of model training, the Recall and IOU obtained by CNN segmentation were remarkably higher than other algorithms ($P < 0.05$).

3.3. Evaluation of the Curative Effect of NPC Radiotherapy Based on CNN. After the radiotherapy, the radiotherapy effect was evaluated by brain MRI images of the patients. Among the 54 NPC patients, 47 cases had no nasopharyngeal local residual, and 7 cases had nasopharyngeal local residual. After manual outlining and judgment by radiologists, there were 38 cases of nasopharyngeal cavity deformation, 44 cases of nasopharyngeal wall thickening (3 cases with parapharyngeal soft tissue thickening), 4 cases of sphenoid wing plate destruction, and 2 cases of slope bone destruction. The thickening of nasopharyngeal wall was

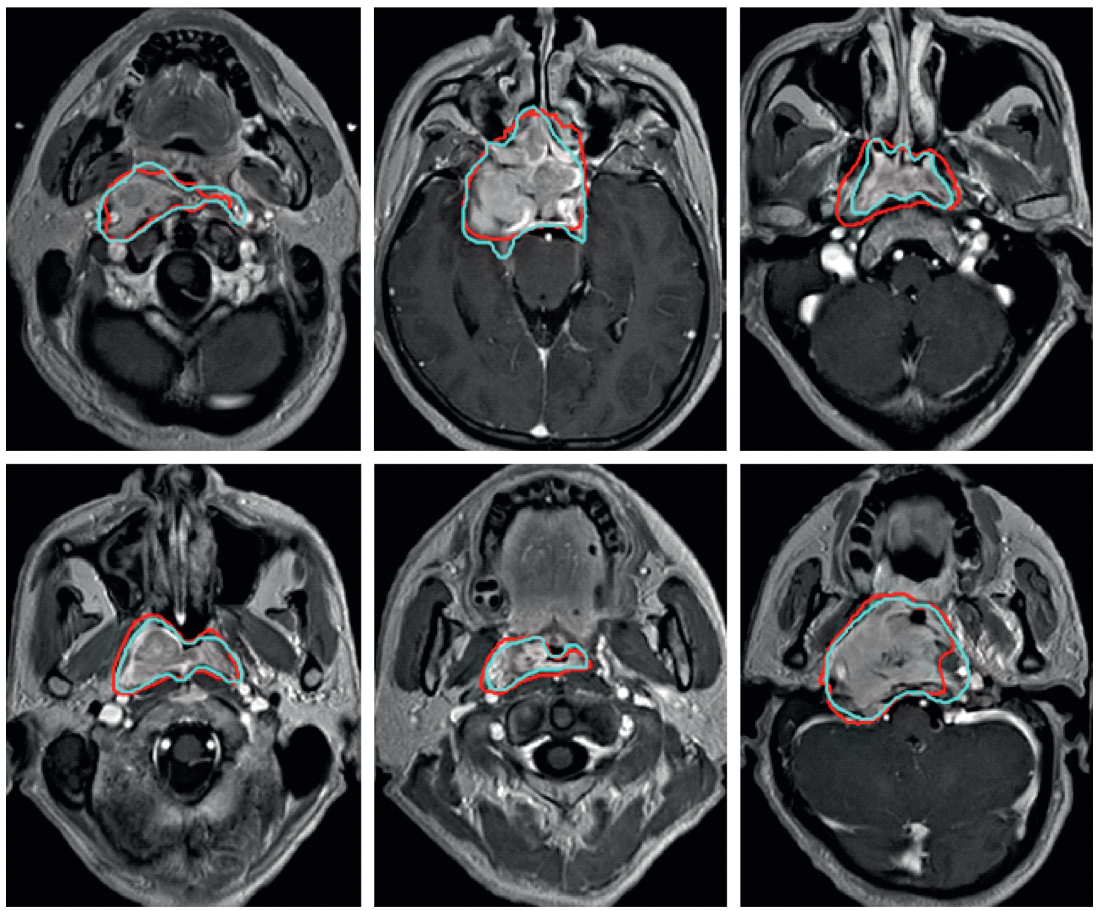

Figure 4: The segmentation effect of CNN on NPC lesions (blue is the area outlined by radiologists, and red is the area automatically segmented by CNN).

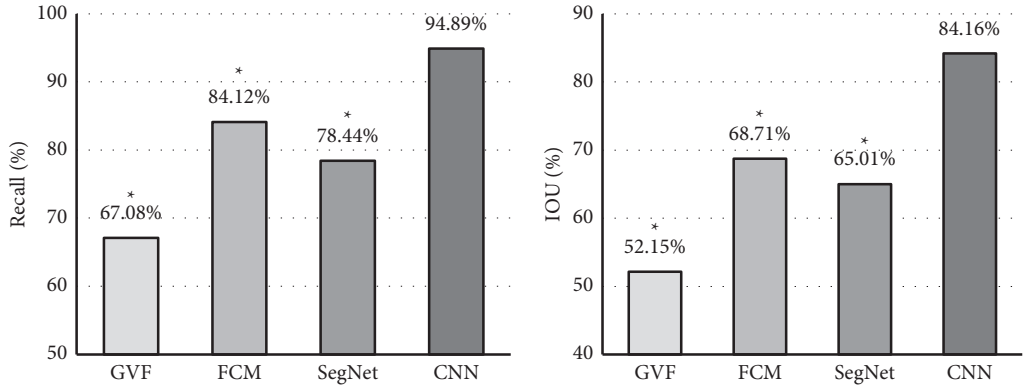

Figure 5: Objective evaluation results based on different algorithms. Note: * indicates $P < 0.05$ as the data were compared with that of CNN.

shown as irregular thickening of nasopharyngeal soft tissue on MRI, and the thickening of parapharyngeal tissue showed slightly high signal (Figure 6). Sphenoid wing plate destruction and slope bone destruction showed partial bone destruction with uneven high intensity on MRI.

After radiotherapy, the ADC of NPC patients was evaluated, and the ADC measured based on different algorithm outlines was compared with the ADC measured by radiologists. The results showed that the ADC measured by CNN for the local residual patients after radiotherapy was 1.108 ± 0.097. For locally residual patients, the ADC measured by CNN was 1.826 ± 0.115 (Figure 7). The measurement result calculated by CNN was relatively closer to the expert manual measurement result, which was statistically different compared with other algorithms ($P < 0.05$).

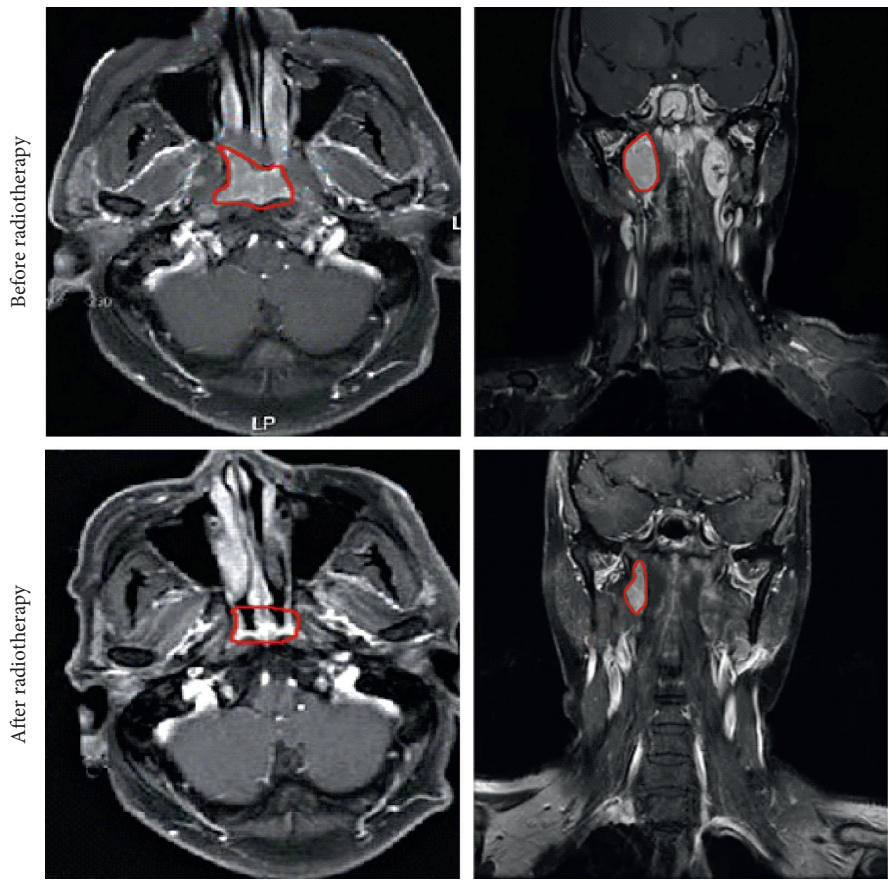

Figure 6: Delineation results of CNN on MRI images of patients after radiotherapy. Note: the patient was a male, aged 51 years.

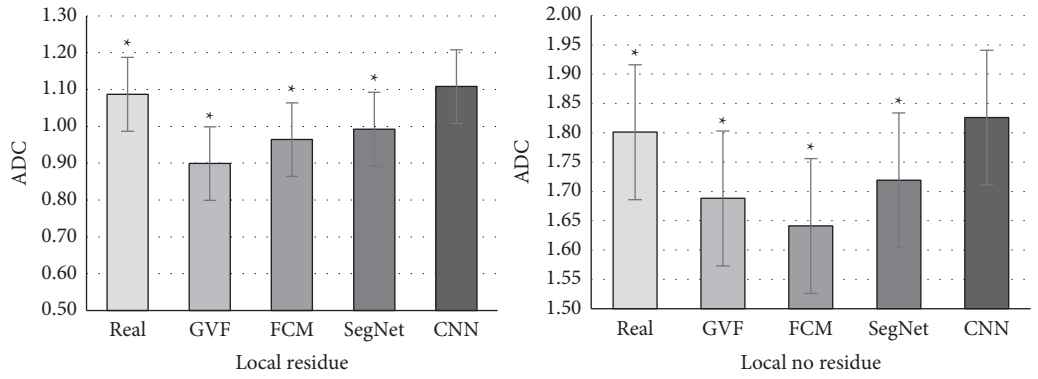

Figure 7: Contrast of ADCs measured based on different algorithms. Note: *indicates $P < 0.05$ with the comparison to the data of CNN.

3.4. Contrast of Coincidence Rate of Postoperative Diagnosis Based on CNN. After 54 NPC patients were treated with radiotherapy, the MRI images of the patients were analyzed for diagnosis. The results showed that 50 patients (92.59%) were accurately diagnosed by CNN for the first time, and 4 patients (7.41%) were missed for the first time (Figure 8). In contrast to other algorithms, the diagnostic accuracy rate was remarkably different ($P < 0.05$). The four cases of missed diagnosis were all patients with skull base invasion, and MRI showed abnormal skull base signals, leading to missed diagnosis.

4. Discussion

The incidence of NPC is the first among head and neck malignant tumors. With the gradual development of radiotherapy technology, the local control rate of NPC has been improved to a certain extent. Patients who receive radiation therapy typically have their lesions completely gone within three months. If the tumor does not disappear six months after surgery, it is residual tumor, and NPC residual or recurrence is the main reason that affects the prognosis and quality of life of patients [21]. Clinical

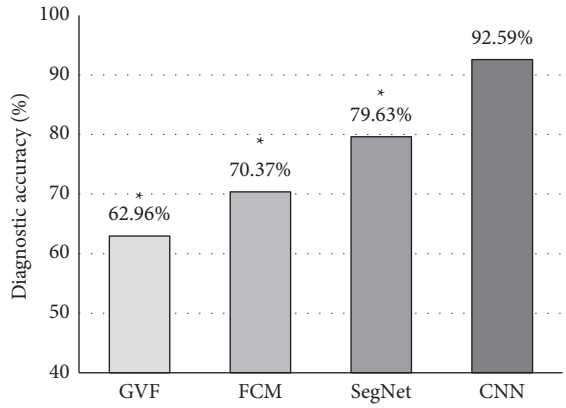

Figure 8: Contrast of diagnostic accuracy based on different algorithms. Note: *indicates $P < 0.05$ with the comparison to CNN data.

imaging examination is still needed for local residual or recurrence of MPC. Currently, CT and MRI are two commonly utilized examination methods. Compared with CT examination, MRI has the omni-directional and multi-parameter characteristics, which can accurately reflect the nerves and blood vessels of the lesion. Thus, MRI can be applied in the efficacy evaluation of NPC radiotherapy [22]. Many quantitative analyses are a segmentation problem. The brightness difference between different parts is not obvious, connected with the surrounding parts, and the boundary is fuzzy. CNN, cyclic neural networks, and generative adversarial networks focus on medical image imaging problems [23]. In recent years, computer-aided medical image analysis has made major breakthroughs in technology and has obvious advantages in improving the efficiency and ability of medical services, which has also become an effective way to solve insufficient medical resources [24].

NPC MRI images were pre-processed, and then CNN was utilized to accurately delineate and segment the lesions in the MRI images of NPC patients. Then, the proposed CNN was compared with the GVF, FCM, and SegNets, and it was found that the Recall and IOU of CNN were 94.89% and 84.16%, respectively. The similarity with the expert's delineation of the lesions was high, suggesting that CNN had ideal segmentation effect on NPC MRI images. Moreover, the MRI images of NPC patients after chemotherapy were analyzed to evaluate the ADC of the patient. ADC is an important way to predict the sensitivity of the tumor to radiotherapy and chemotherapy and whether the tumor remains in recurrence. The higher the ADC, the better the anti-tumor treatment effect. It was found that for patients with local residual tumors and local residual tumors after radiotherapy, the ADCs measured by CNN were 1.108 ± 0.097 and 1.826 ± 0.115, respectively. These data were in line with the manual measurement results of experts. The results were in line with the study of Peng et al. [25]. Diagnosis of patients after surgery suggested that the diagnostic accuracy of CNN was 92.59%, which was remarkably different from the other three algorithms ($P < 0.05$), suggesting ideal diagnostic effect of CNN on radiotherapy efficacy.

5. Conclusion

CNN was utilized to outline and segment the lesion sites on NPC MRI images, and the NPC radiotherapy efficacy was judged by MRI images. It was proved that CNN could identify the lesion sites on MRI images of NPC patients and accurately evaluate the radiotherapy effect of patients. The algorithm presented in this study can assist clinicians, which is suitable to be applied in imaging diagnosis of NPC patients. It can be concluded that MRI based on CNN yielded high clinical adoption value for evaluation of the NPC radiotherapy effect on patients. However, there are still some deficiencies in this study, which are manifested as a small number of included cases and that the truth all patients within six months of radiotherapy were just confirmed by biopsy pathology without long-term follow-up, which needs to be further studied by increasing the sample size in future studies.

Data Availability

The data used to support the findings of this study are available from the corresponding author upon request.

Conflicts of Interest

The authors declare no conflicts of interest.

Authors' Contributions

Haifeng Qian and Yancheng Fang contributed equally to this work.

References

[1] R. Guo, Y.-P. Mao, L.-L. Tang, L. Chen, Y. Sun, and J. Ma, "The evolution of nasopharyngeal carcinoma staging," *The British Journal of Radiology*, vol. 92, no. 1102, Epub 2019 Jul 12. PMID: 31298937; PMCID: PMC6774596, Article ID 20190244, 2019 Oct.

[2] X.-S. Sun, X.-Y. Li, Q.-Y. Chen, L.-Q. Tang, and H.-Q. Mai, "Future of radiotherapy in nasopharyngeal carcinoma," *The British Journal of Radiology*, vol. 92, no. 1102, Epub 2019 Jul 9. PMID: 31265322; PMCID: PMC6774595, Article ID 20190209, 2019.

[3] M. L. Sandler, J. R. Sims, M. H. Xing et al., "Atypical metastasis of nasopharyngeal cancer: noncontiguous spread to the ipsilateral ear," *Clinical Imaging*, vol. 72, pp. 70–74, 2021, Epub 2020 Nov 14. PMID: 33217673.

[4] Z.-G. Liang, H. Q. Tan, F. Zhang et al., "Comparison of radiomics tools for image analyses and clinical prediction in nasopharyngeal carcinoma," *The British Journal of Radiology*, vol. 92, no. 1102, Epub 2019 Aug 27. PMID: 31453720; PMCID: PMC6774600, Article ID 20190271, 2019.

[5] U. Akbas, C. Koksal, N. D. Kesen, K. Ozkaya, H. Bilge, and M. Altun, "Nasopharyngeal carcinoma radiotherapy with hybrid technique," *Medical Dosimetry*, vol. 44, no. 3, pp. 251–257, 2019, Epub 2018 Oct 23. PMID: 30366620.

[6] C. H. Chapman, U. Parvathaneni, and S. S. Yom, "Revisiting induction chemotherapy before radiotherapy for head and neck cancer, part II: nasopharyngeal carcinoma," *Future Oncology*, vol. 13, no. 7, pp. 581–584, 2017, PMID: 28169580.

[7] W. Zhang, Q. Guo, G. Liu et al., "NKILA represses nasopharyngeal carcinoma carcinogenesis and metastasis by NF-κB pathway inhibition," *PLoS Genetics*, vol. 15, no. 8, PMID: 31430288; PMCID: PMC6716677, Article ID e1008325, 2019.

[8] W. T. Ng, J. Corry, J. A. Langendijk et al., "Current management of stage IV nasopharyngeal carcinoma without distant metastasis," *Cancer Treatment Reviews*, vol. 85, 2020 Epub 2020 Feb 21. PMID: 32113080, Article ID 101995.

[9] S. Ak, C. Kiliç, and S. Özlügedik, "Correlation of PET-CT, MRI and histopathology findings in the follow-up of patients with nasopharyngeal cancer," *Brazilian Journal of Otorhinolaryngology*, vol. 87, pp. 643–648(6), 2021, Epub ahead of print. PMID: 31982379.

[10] G. Spadarella, G. Calareso, E. Garanzini, L. Ugga, A. Cuocolo, and R. Cuocolo, "MRI based radiomics in nasopharyngeal cancer: systematic review and perspectives using radiomic quality score (RQS) assessment," *European Journal of Radiology*, vol. 140, 2021 Epub 2021 Apr 30. PMID: 33962253, Article ID 109744.

[11] J. Y. Yu, D. Zhang, X. L. Huang et al., "Quantitative analysis of DCE-MRI and RESOLVE-DWI for differentiating nasopharyngeal carcinoma from nasopharyngeal lymphoid hyperplasia," *Journal of Medical Systems*, vol. 44, no. 4, p. 75, 2020 PMID: 32103352.

[12] J. Mao, J. Fang, X. Duan et al., "Predictive value of pretreatment MRI texture analysis in patients with primary nasopharyngeal carcinoma," *European Radiology*, vol. 29, no. 8, pp. 4105–4113, 2019, Epub 2019 Jan 7. PMID: 30617473; PMCID: PMC6610272..

[13] M. Beigi, A. F. Kazerooni, M. Safari et al., "Heterogeneity analysis of diffusion-weighted MRI for prediction and assessment of microstructural changes early after one cycle of induction chemotherapy in nasopharyngeal cancer patients," *La radiologia medica*, vol. 123, no. 1, pp. 36–43, 2018, Epub 2017 Sep 15. PMID: 28914416.

[14] K. Meng, J. Tey, F. C. H. Ho, H. Asim, and T. Cheo, "Utility of magnetic resonance imaging in determining treatment response and local recurrence in nasopharyngeal carcinoma treated curatively," *BMC Cancer*, vol. 20, no. 1, p. 193, 2020 PMID: 32143592; PMCID: PMC7060635..

[15] X. Yang, X. Li, X. Zhang, F. Song, S. Huang, and Y. Xia, "[Segmentation of organs at risk in nasopharyngeal cancer for radiotherapy using a self-adaptive Unet network]," *Nan Fang Yi Ke Da Xue Xue Bao*, vol. 40, no. 11, pp. 1579–1586, 2020, Chinese PMID: 33243744; PMCID: PMC7704375.

[16] X. Ming, R. W. Oei, R. Zhai et al., "MRI-based radiomics signature is a quantitative prognostic biomarker for nasopharyngeal carcinoma," *Scientific Reports*, vol. 9, no. 1, p. 10412, 2019 PMID: 31320729; PMCID: PMC6639299..

[17] S. Guo, R. Chen, H. Li, T. Zhang, and Y. Liu, "Identify severity bug report with distribution imbalance by CR-SMOTE and ELM," *International Journal of Software Engineering and Knowledge Engineering*, vol. 29, no. 2, pp. 139–175, 2019.

[18] L. Lin, Q. Dou, Y.-M. Jin et al., "Deep learning for automated contouring of primary tumor volumes by MRI for nasopharyngeal carcinoma," *Radiology*, vol. 291, no. 3, pp. 677–686, 2019, Epub 2019 Mar 26. PMID: 30912722.

[19] L. M. Wong, A. D. King, Q. Y. H. Ai et al., "Convolutional neural network for discriminating nasopharyngeal carcinoma and benign hyperplasia on MRI," *European Radiology*, vol. 31, no. 6, pp. 3856–3863, 2021, Epub 2020 Nov 25. PMID: 33241522.

[20] Z. Ma, S. Zhou, X. Wu et al., "Nasopharyngeal carcinoma segmentation based on enhanced convolutional neural networks using multi-modal metric learning," *Physics in Medicine & Biology*, vol. 64, no. 2, PMID: 30524024, Article ID 025005, 2019.

[21] A. W. M. Lee, W. T. Ng, J. Y. W. Chan et al., "Management of locally recurrent nasopharyngeal carcinoma," *Cancer Treatment Reviews*, vol. 79, 2019 Epub 2019 Aug 21. PMID: 31470314, Article ID 101890.

[22] B. Zhang, J. Tian, D. Dong et al., "Radiomics features of multiparametric MRI as novel prognostic factors in advanced nasopharyngeal carcinoma," *Clinical Cancer Research*, vol. 23, no. 15, pp. 4259–4269, 2017, Epub 2017 Mar 9. PMID: 28280088.

[23] P. Naveen and P. Sivakumar, "Adaptive morphological and bilateral filtering with ensemble convolutional neural network for pose-invariant face recognition," *Journal of Ambient Intelligence and Humanized Computing*, vol. 12, no. 3, pp. 10023–10033, 2021.

[24] P. Naveen, "A deep convolution neural network for facial expression recognition," *Journal of Current Science and Technology*, vol. 11, no. 3, pp. 402–410, 2021.

[25] H. Peng, D. Dong, M.-J. Fang et al., "Prognostic value of deep learning PET/CT-Based radiomics: potential role for future individual induction chemotherapy in advanced nasopharyngeal carcinoma," *Clinical Cancer Research*, vol. 25, no. 14, pp. 4271–4279, 2019, Epub 2019 Apr 11. PMID: 30975664.